analytical chemistry

Article

pubs.acs.org/ac

DNA Domino-Based Nanoscale Logic Circuit: A Versatile Strategy for Ultrasensitive Multiplexed Analysis of Nucleic Acids

Hadi Ravan,* Mojdeh Amandadi, and Saeed Esmaeili-Mahani

Department of Biology, Faculty of Science, Shahid Bahonar University of Kerman, Kerman, Iran 7616914111

Supporting Information

ABSTRACT: In recent years, the analytical application of logical nanodevices has attracted much attention for making accurate decisions on molecular diagnosis. Herein, a DNA domino-based nanoscale logic circuit has been constructed by integrating three logic gates (AND-AND-YES) for simultaneous analysis of multiple nucleic acid biomarkers. In the first AND gate, a chimeric target DNA comprising of four biomarkers was hybridized to three biomarker-specific oligonucleotides (TRs) via their 5′-end regions and to a capture probe-magnetic microparticle. After harvesting the complex, 3′ overhang regions of the TRs were labeled with three distinct monolayer double-stranded (ds) DNA-gold nanoparticles (DNA-AuNPs). Upon gleaning the complex and addition of initiator oligonucleotide, a series of toehold-mediated strand displacement reactions, which are reminiscent of a domino chain, spontaneously occurred between the confined dsDNAs on the nanoparticles' surface in the second AND gate. The output of the second gate entered into the last gate and triggered an exponential hairpin assembly to form four-way junction nanostructures. The resulting nanostructures bear split parts of DNAzyme at each end of the four arms which, in the presence of hemin, form catalytic hemin/G-quadruplex DNAzymes with peroxidase activity. The smart biosensor has exhibited a turn-on signal when all biomarkers are present in the sample. In fact, should any of the biomarkers be nonexistent, the signal remains turned-off. The biosensor can detect the biomarkers with a LOD value of 100 aM and a noticeable capability to discriminate single-nucleotide substitutions.

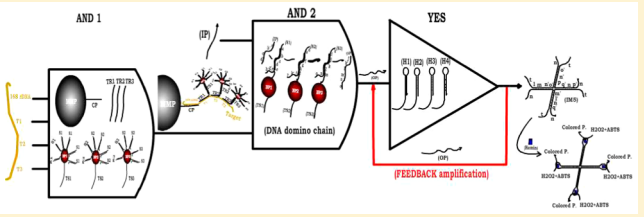

Downloaded via UNIV OF SOUTH DAKOTA on July 12, 2018 at 08:45:30 (UTC).
See https://pubs.acs.org/sharingguidelines for options on how to legitimately share published articles.

To enhance the accuracy of diagnoses, physicians exploit multiplex processing platforms to interrogate more than one biomarker simultaneously in each specimen. Because of the complexity of biological systems, single biomarker alone is not effective enough for an authentic diagnosis.[1] Multiplexed analysis of nucleic acids is usually performed by such techniques as multiplex PCR,[2] multiplex mini-sequencing,[3] multiplex ligation-dependent probe amplification (MLPA),[4] and DNA microarray.[5] Despite the high reliability of these methods, they are costly, time-consuming, and not responsive to all clinical demands. Moreover, a certain variety of these platforms calls for special attention for primer design due to their target-based amplification nature. Alternative approaches, such as multiplexed DNA biobarcodes[6] and multiplexed Nanoflares, meet these purposes through applying the principle of enzyme-free bioassay strategies.[7−10] However, the dissociation of biobarcode DNAs from their fastened floor may require time-consuming chemical treatments or application of toxic reagents.[11] On the other hand, although Nanoflares have provided a promising biosensing platform for in vivo multiplex RNA analysis, sensitivity issues limited utilizing this nanodevice for in vitro detection. In this respect, there is a great demand for systems that enable multiplex analysis of nucleic acids in biological relevant concentrations.

Taking a new look from biocomputing standpoint, a multiplex assay is constructed based on Boolean logic operations that offer a unique output signal in response to several biomarker inputs.[8,12−15] In recent years, a variety of innovative enzyme-free DNA-based logic nanodevices has been designed for multiplex analysis of nucleic acids. For example, Winfree's group constructed a "seesaw" gate, based on programmed toehold-mediated DNA strand displacement (TMSD) reactions, to encode Boolean values in response to multiple nucleic acid inputs.[16] By the same strategy, Hemphill and co-workers engineered a series of DNA logic gates to respond to various microRNAs in living cells.[17] Moreover, Liu and co-workers have designed an aptasensor based on the specific interaction between graphene oxide and fluorophore-labeled DNA strands for multiplexed analysis of nucleic acids.[18] Using electrochemical logic devices, Kang et al. developed multiplexed biosensor for analysis of different genetic biomarkers.[19] Recently, Pu and Liu have, respectively, implemented "molecular keypad lock" and "full-subtractor" arithmetic logic operations that have the potential to contribute in multiplex analysis of nucleic acids.[20−22]

Besides the approaches described above, colorimetric-based DNA computing has attracted a growing interest for the design of smart nanodevices.[14,23−26] Of particular interest has been a stratum of these platforms that incorporate G-quadruplex DNAzymes into the logic circuits due to their modular and dynamic behaviors toward various stimuli. For example, efforts

Received: February 17, 2017
Accepted: May 1, 2017
Published: May 1, 2017

 © 2017 American Chemical Society

DOI: 10.1021/acs.analchem.7b00607
Anal. Chem. 2017, 89, 6021−6028

Scheme 1. Schematic Design Strategy for the DNA Domino-Based Nanodevice[a]

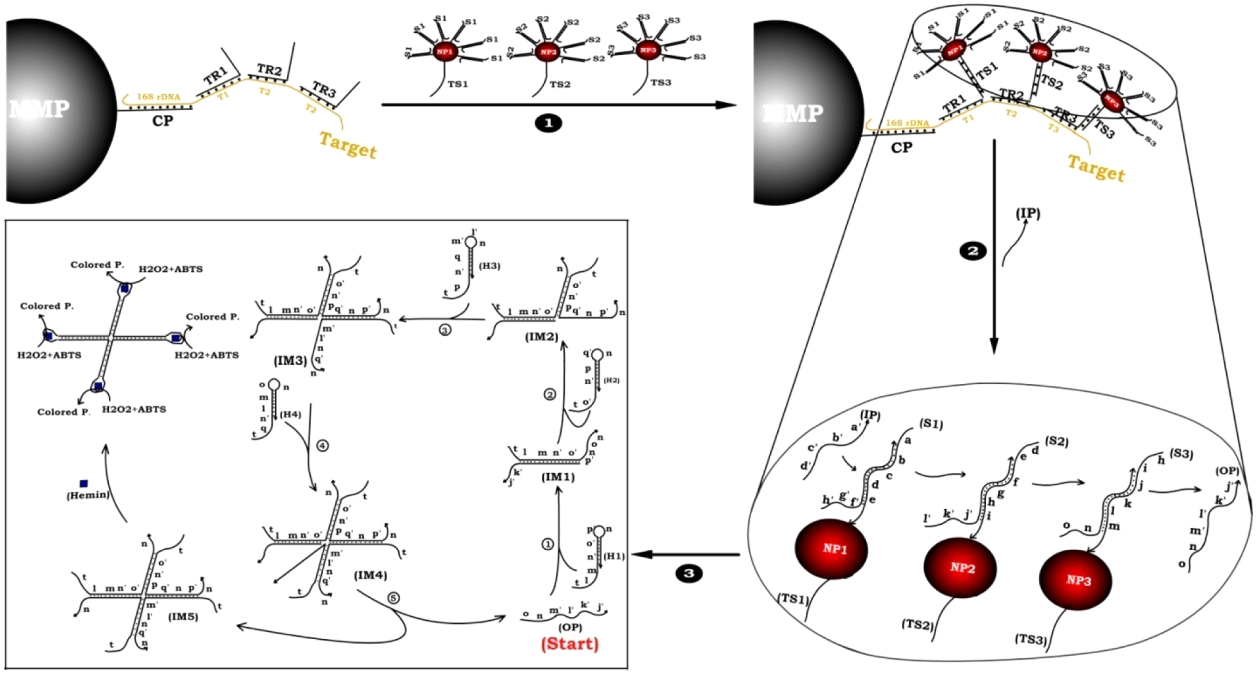

[a]Capture probe, CP; magnetic microparticle, MMP; biomarker-specific oligonucleotides, TR1, TR2, and TR3; DNA-AuNPs, NP1, NP2 and NP3; hairpins, H1, H2, H3, and H4.

Scheme 2. Representation of AND-AND-YES Concatenated Logic Circuit[a]

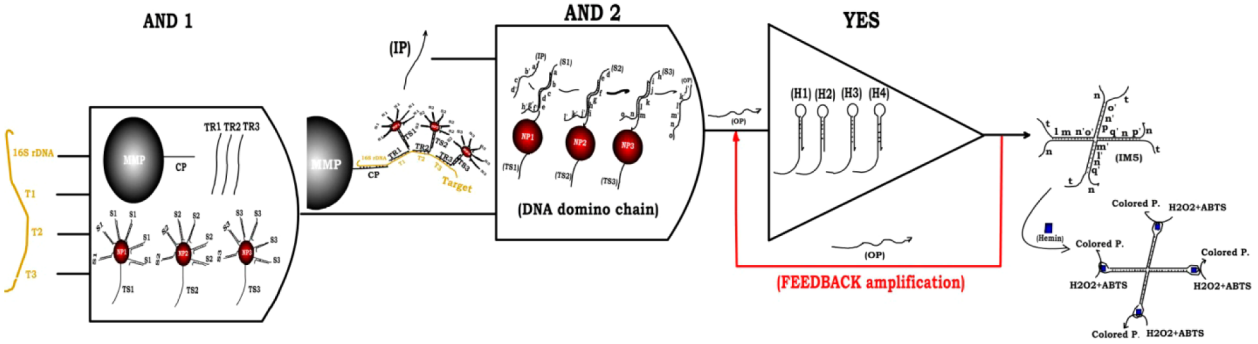

[a]The logic circuit is run by 16S rDNA, T1, T2 and T3 biomarkers as input. The first AND gate (AND 1) is composed of MMP-CP, three biomarker-specific oligonucleotides (TR1, TR2, and TR3), and three DNA-AuNPs. The output signal of AND 1 and IP strand serve as inputs for second gate (AND 2) and activates TMSD reaction in this gate. OP strand generated by AND 2 gate is utilized as the input for the last YES gate and runs the exponential hairpin assembly in this gate. The output IM4 is formed and released OP strand, triggers feedback amplification loop. Upon incubation of the system with hemin, G-quadruplex DNAzymes are formed on the DNA four-way junctions. The DNAzymes catalyze the H_2O_2-mediated oxidation of ABTS for generation of a colorimetric signal.

from Wang's group have led to the construction of several logic devices based on the formation of an active peroxidase-mimicking G-quadruplex DNAzyme from their spilt partzymes in response to different input DNAs.[27] Geo and co-workers successfully established a series of colorimetric logic gates based on triplex-helix molecular switch machines and G-quadruplex DNAzyme.[28] However, since these nanodevices have been developed to imitate the function of semiconductor-based computing, the improvement of certain sensing parameters like sensitivity has been left underrepresented. To boost the efficiency of these gadgets for intelligent diagnoses, signal amplification capability, as a prerequisite for enhancing sensitivity, must be integrated in these platforms. In this respect, Chen and co-workers have constructed a three-way concatenated DNA nanostructure performing colorimetric logic operations, as a biocomputing keypad lock security system, in response to a single DNA biomarker input.[29] In a variation of this theme, Xiang's group has successfully developed "DNAzyme ferris wheel" nanostructure for singleplex and colorimetric detection of miR-141 biomarker.[30] To explore new dimensions of nanostructure-based detection, developing DNA-based logic devices that offer ultrasensitive colorimetric sensing platforms for simultaneous analysis of several nucleic acids seems worthy of effort.

In this work, a new colorimetric logic operation has been implemented based on DNA domino-induced four-way G-quadruplex junctions for a highly sensitive and specific simultaneous detection of multiple nucleic acid biomarkers.

DOI: 10.1021/acs.analchem.7b00607
Anal. Chem. 2017, 89, 6021−6028

This biocomputing nanodevice executes as a concatenated logic circuit with an enzyme-free signal amplification capability, which is composed of three sequential logic gates (AND-AND-YES) to respond to multiple biomarker inputs. As shown in Schemes 1 and 2, the first AND gate is a DNA hybridization-translating gadget that donates multiple-input recognition and signal amplification capabilities to the biosensor. The second AND gate serves as a TMSD-based DNA domino chain which offers an intelligent multiplexing capability to the biosensor. The output of the last AND gate (OP) enters into final logic gate (YES) and activates a feedback amplification loop in a DNA hairpin assembly process to further improve the output signal. Overall, the logical biosensor has exploited the signal amplification capability of three famous platforms, including (i) gold nanoparticle (AuNP)-assisted signal amplification, which is achieved through translating a single DNA hybridization event into a monolayer DNA-modified AuNP (DNA-AuNP) by the first AND gate, (ii) nanostructure-assisted signal amplification, which is obtained out of the formation of DNA nanostructures by an exponential hairpin assembly through the last gate (YES), and (iii) DNAzyme-assisted signal amplification, which is earned by the signal enhancement capability of peroxidase-mimicking G-quadruplex DNAzymes, to sensitively detect multiple DNA biomarkers at attomolar levels (aM = 10^{-18} M).

EXPERIMENTAL SECTION

Materials and Reagents. All DNA oligonucleotides (HPLC and PAGE purified) were synthesized by Bioneer Co. (South Korea) and the sequences of which are represented in Table S1. Dynabeads MyOne carboxylic acids (carboxylate-modified magnetic microparticles, MMPs) with a diameter of 1 μm were obtained from Invitrogen. The 30 nm-AuNP stabilized in citrate buffer, dithiothreitol (DTT), 2-(*N*-morpholino)ethanesulfonic acid (MES) buffer, *N*-(3-(dimethylamino)propyl)-*N*′-ethyl-carbodiimide hydrochloride (EDC), Tween-20, Tris(hydroxymethyl)aminomethane, ethylenediaminetetraacetic acid disodium salt (EDTA), hemin, and 2,2′-azino-bis(3-ethylbenzothiazoline-6-sulfonicacid) (ABTS) were achieved from Sigma-Aldrich Co. 4-(2-Hydroxyethyl)-1-piperazineethanesulfonic acid (HEPES) and H_2O_2 were purchased from Bio Basic Inc. (Canada). All other reagents were of analytical grade.

Bacterial Culture, Enumeration, and DNA Extraction. Bacterial strains including *E. coli* O157:H7, *E. coli* O55:H7, *E. coli* O145, and *S. typhimurium* were picked from MacConkey plates and inoculated in tryptic soy broth at 37 °C. After 16 h incubation, each bacterial suspension was serially diluted in phosphate-buffered saline, pH 7.4 (PBS), and utilized either for colony counting by plating on a suitable growth medium or for extracting DNA by the boiling method at 95 °C.[31]

Oligonucleotide Design Strategy. In order to evaluate the efficiency of the biosensor for multiplex analysis of nucleic acids, we sought for four special biomarkers in *E. coli* O157:H7 genome, of which three were present in *E. coli* O55:H7, two in *E. coli* O145, and one in *S. typhimurium* genomes. After *in silico* comparison of the four bacterial genomes, we opted four nucleotide regions from *eae* (T1), *rfbE* (T2), *fliC* (T3), and 16S rDNA genes that met all the above criteria. On the basis of the selected regions, a chimeric target DNA was designed in which the biomarkers were joined by a dinucleotide TT for enhancing the hybridization reaction. To verify the discrimination ability of the biosensor, three spurious chimeric targets were also designed with each possessing a single nucleotide substitution (SNS) in each biomarker (Table S1). A 5′-NH_2-terminated capture probe (CP) that is complementary to 16S rDNA biomarker has been designed for loading on MMPs. Three biomarker-specific oligonucleotides (TR1, TR2, and TR3) were designed serving as the complementary to the biomarkers T1, T2, and T3, respectively. Each biomarker-specific oligonucleotide bears an overhang region at its 3′end that is complementary to its corresponding TS oligonucleotide. Three types of oligonucleotide-functionalized AuNPs were constructed using 3′-thiol-modified S (S1, S2, and S3) and 5′-thiol-modified TS (TS1, TS2, and TS3) oligonucleotides. Three sequences CS1, CS2, and CS3 were hybridized to different S oligonucleotides (Table S1). In order to initiate the domino reaction by DNA duplexes formed on the surface of AuNPs (S|CS duplexes), an initiator probe (IP), which was complementary to the S1 strand, was designed. Four hairpin structures (H1, H2, H3, and H4) were selected as a building block for the construction of four-way junctions. Each hairpin sequence was flanked by two G-rich fragments of 3:1 split G-quadruplex at its 5′- and 3′-ends, respectively (Table S1). Domains of sequences used in this study are represented in Table S2.

Preparation of Monolayer DNA-AuNP. To reduce the disulfide bound of the alkanethiol oligonucleotides, the oligonucleotides were incubated with 1.0 N DTT in 0.01 M sodium acetate (pH 5.2) for 15 min at room temperature and then extracted three times with ethyl acetate. The freshly reduced thiol-modified oligonucleotides (a mix of S and TS oligonucleotides, with a ratio of 100:1) in a final concentration of 8 μM were combined with AuNP solution. To the solution, sodium phosphate buffer containing 0.1% SDS was added in a final concentration of 9 mM (pH 7.0) and gently shook in the dark for 30 min. The mixture was slowly brought up to concentrations of 0.1, 0.2, and 0.3 M sodium chloride within 4 h intervals and then incubated overnight at room temperature. The solution was centrifuged at 13 000 rpm for 30 min, and the precipitate was redispersed in 9 mM sodium phosphate buffer containing 0.3 M sodium chloride and 0.01% SDS. The final step was repeated several times to obtain the purified oligonucleotide-AuNP conjugates. The complementary counterparts (CS) of the S oligonucleotides were added to the purified oligonucleotide-AuNP in the final concentration of 6 μM. The solution was heated to 65 °C, slowly cooled down to 25 °C at the rate of 0.01 °C/min, and stored in this temperature for 2 h. Finally, the solution was centrifuged and the precipitate was suspended in 9 mM sodium phosphate buffer containing 0.3 M sodium chloride, 0.01% SDS. This step was repeated three times to refine the precipitate.

DNA-Modified MMP Preparation. The carboxylate MMPs were functionalized with 5′-NH_2-terminated capture probes using the protocol suggested by the manufacturer with some modifications. A volume of 1 mL of MMP was magnetically collected and washed twice in 100 mM MES buffer (pH 4.8) for 10 min. 5′-NH_2-terminated oligonucleotides (50 nmol) was added to the MMPs in MES buffer and incubated for 30 min at room temperature with slow end-overend rotation (SER). To the suspension, 0.469 M EDC in cold MES buffer was added and incubated overnight at 4 °C with SER. To quench the unreacted activated carboxylic acid of the MMPs, 250 mM Tris buffer (pH 7.5) containing 0.01% tween-20 was added to the solution for 30 min. The MMPs

DOI: 10.1021/acs.analchem.7b00607
Anal. Chem. 2017, 89, 6021−6028

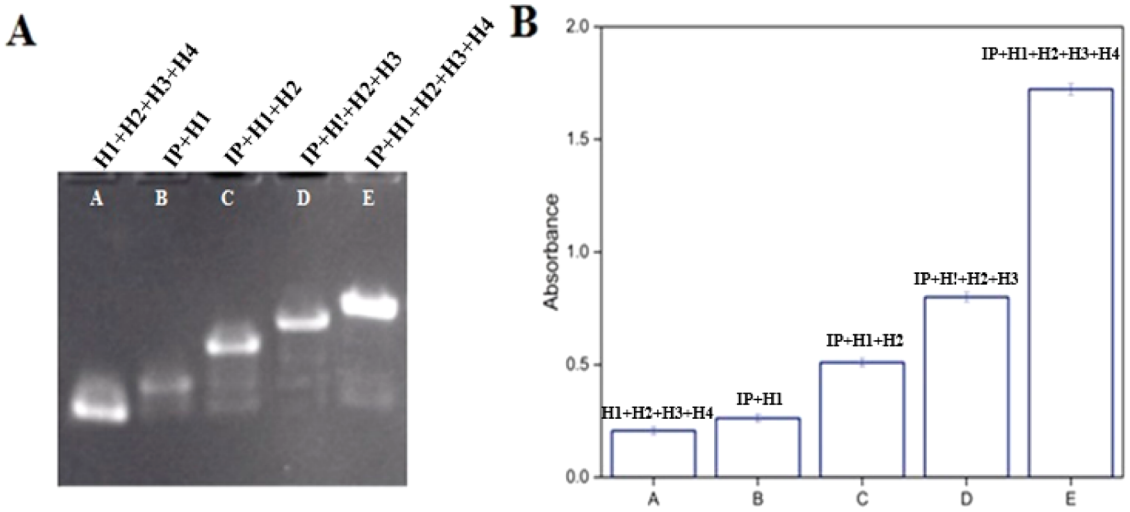

Figure 1. (A) 2% agarose gel electrophoresis demonstrating the DNA domino-based circuit in several analyzing reactions (in presence/absence of different hairpins and IP strand) based on the formation of branched junction nanostructures. (B) Corresponding absorbance intensity of the system at 414 nm in several analyzing reactions (in presence/absence of different hairpins and IP strand).

were rinsed twice with 10 mM Tris-EDTA buffer, resuspended in the same buffer, and stored at 4 °C.

DNA Domino-Induced Four-Way Junction Protocol. In a typical DNA domino assay, a 50-μL target DNA (different concentrations) was mixed with 7 μL of MMPs and 3 μL of the biomarker-specific oligonucleotides (TR1, TR2, and TR3). To the solution, 340 μL of Tris-buffered saline (TBS) (10 mM Tris, 90 mM NaCl, 2.7 mM $MgCl_2$, pH 7.5) was added in order that the final concentrations of TR1, TR2, and TR3 reach to 1000 nM, 800 nM, and 350 nM, respectively. The solution was heated to 95 °C for 1 min, cooled down to 55 °C, and incubated in the same temperature for 30 min with gentle shaking. After being harvested by magnetic field, the complex was washed three times with TBS containing 0.01% tween-20. To the complex, 100 μL of each monolayer DNA-AuNP was added and incubated for 30 min with gentle shaking. After harvesting and washing the complex, 100 μL of TBS solution (contain 2 μM of each hairpin [H1, H2, H3, and H4] and 2 μM IP strand) was added and incubated at 25 °C. After 120 min incubation, the complex was harvested by a magnetic field and the supernatant was used for the next experiments (gel electrophoresis and colorimetric evaluations). For colorimetric evaluation, 100 μL of hemin in HEPES buffer (6 mM hemin, 50 mM HEPES, 40 mM KCl, 400 mM NaCl, 0.1% Triton X-100, and 2% DMSO) was added to the supernatant and incubated at 25 °C for 40 min. The peroxidation reaction was started by adding 2 mM ABTS and 2 mM H_2O_2 and incubated for 15 min. After transferring 200 μL of the solution into each microwell, the absorbance intensity was measured at 414 nm using a BioTek microtiter plate reader.

RESULTS AND DISCUSSION

Design and Working Principle of the DNA Domino-Based Nanodevice. The configuration of DNA domino-based nanoscale logic circuit along with its operation is schematically illustrated in Schemes 1 and 2. By the first AND gate, a chimeric target DNA containing four biomarkers (16S rDNA, T1, T2, and T3) has been anchored to a CP-MMP through the complementary interaction with 16S rDNA biomarker. Concomitantly, the biomarkers T1, T2, and T3 have been hybridized to three biomarker-specific oligonucleotides (TR1, TR2, and TR3) each of which independently bears an overhang region with DNA hybridization-translation activity.[32] Upon hybridization, the biomarker-specific oligonucleotides have been labeled with three distinct monolayer double-stranded (ds) DNA-AuNPs via TS1, TS2, and TS3. Afterward, by entrance of "IP" strand, a series of DNA strand displacement reactions, which are reminiscent of a domino chain reaction, have spontaneously occurred between the confined dsDNAs on the nanoparticles' surface in the second AND gate. In this gate, IP strand uses the domain a′ as a toehold to hybridize to the exposed domain a of S1 strand, potentially initiating TMSD reaction to release its complementary counterpart CS1. Subsequently, the newly exposed e′−d′ toehold binds to their complementary domains on S2 and initiates a new strand displacement reaction to release CS2. Analogously, the newly accessible toehold of CS2 (i′−h′) initiates another branch migration reaction to release CS3 strand as output of the second AND gate (OP). OP strands serve as input for the last gate (YES) and catalyze a cascade of DNA self-assembly steps to form four-way branched junctions in the presence of a set of DNA hairpins (H1−H4) (Scheme 1). Upon arrival of OP, a DNA nucleation reaction would occur between domain m′−l′ of OP and its complementary region on the H1 hairpin. By a DNA strand displacement reaction, the stem of H1 is then opened and IM1 is generated. By the same reaction, H2, H3, and H4 hairpins are unwound, and IM2, IM3, and IM4 intermediates are, respectively, produced. The inherent instability of IM4 complex causes that the OP strand is released from the complex and participates in a feedback amplification loop to produce more DNA four-way junction nanostructures. The resulting nanostructures bear split parts of DNAzyme at each end of the four arms that, in the presence of hemin, form catalytic hemin/G-quadruplex DNAzymes with peroxidase activity. We can see that the intelligent multiplexing capability of the system is achieved by implementing a well-designed DNA domino chain in the second AND gate. Lack of each biomarker disrupts this domino chain, whereby the OP strand is not released at the end, and thus no signal output is produced. Taken together, the smart biosensor has exhibited a turn-on signal when all biomarkers are present in the sample.

DOI: 10.1021/acs.analchem.7b00607
Anal. Chem. 2017, 89, 6021−6028

As a matter of fact, should any of the biomarkers are nonexistent, the signal remains turned-off.

Mechanism Demonstration by Gel Electrophoresis and Colorimetric Evaluations. Because of the short and similar length of input and output oligonucleotides contributing to the domino chain reaction (IP, CS1, CS2, OP), verification of the DNA domino reaction is not directly assessable by gel electrophoresis. However, since the formation of final products (four-way junction structures) is entirely dependent on the formation of MMP-target-AuNP complex and the occurrence of DNA domino chain reaction between the confined dsDNAs on the AuNPs, the feasibility of the DNA domino reaction could be validated based on "the formation of branched junction nanostructures" by gel electrophoresis and absorbance spectrophotometry. For this purpose, several analyzing reactions were conducted based on the standard DNA domino-induced four-way junction protocol with some modifications which are as follows. Briefly, the target DNA was mixed with CP-MMP and biomarker-specific oligonucleotides (TR1, TR2, and TR3). The formed complex was harvested by a magnetic field and washed. The monolayer DNA-AuNPs were added to the complex and incubated for 30 min. After harvesting and washing the new formed complex, several reactions were conducted in the presence/absence of different hairpins and IP strand which are as follows:

(i) The complex was incubated with all DNA hairpins (H1, H2, H3, and H4) in the absence of IP strand (lane A and bar A in parts A and B of Figure 1, respectively).

(ii) The complex was incubated with H1 hairpin and IP strand (lane B and bar B).

(iii) The complex was incubated with H1 and H2 hairpins and IP strand (lane C and bar C).

(iv) The complex was incubated with H1, H2, and H3 hairpins and IP strand (lane D and bar D).

(v) The complex was incubated with H1, H2, H3, and H4 hairpins and IP strand (lane E and bar E).

After 120 min incubation, the MMP-target-AuNP complex was harvested by a magnetic field and the "supernatant" was used for gel electrophoresis and colorimetric evaluations. The results of gel electrophoresis showed that the electrophoretic mobility of the products was completely consistent with our prediction for DNA domino chain reaction. As displayed in Figure 1A, in this condition, the electrophoretic mobility of the reaction product yielded a characteristic band corresponding to unassembled hairpins and barely formed an intermediate product (lane A in Figure 1A). This result implies that the hairpins could coexist in the system with no self-assembly in the absence of IP strand. Upon introduction of IP to the system containing solely H1, the mobility decreases due to the formation of IM1 (in Scheme 1) (lane B in Figure 1A). The addition of H2, H3, and H4 to the system gradually results in the formation of complexes (IM2, IM3, and IM4) with lower mobility (lanes C, D, and E), respectively. To further verify the feasibility of the functional DNAzyme nanostructures for performing colorimetric logic operation, UV−visible absorbance of different mixtures was investigated. As shown in Figure 1B, the coexistence of H1−H4 in the solution without IP introduction exhibits a weak characteristic absorbance peak at 414 nm (the background signal of ABTS-H_2O_2 substrate) (bar A). By the introduction of IP into the solution, containing only H1, the absorbance bar (bar B) showed almost no change relative to bar A. This result confirms that the produced IM1 complex (in Scheme 1) could not draw intact DNAzyme nanostructures. Further addition of H2 and H3 to the system gradually increases the absorbance intensity (bar C and D in Figure 1B), respectively. Such an increase was related to the formation of functional DNAzymes on the IM2 and IM3 complexes. The catalytic self-assembly of H1−H4 in the presence of IP critically increased the absorbance intensity (approximately 210% when compared with the mixture containing IP, H1, H2, and H3). The result could be a consequence of the cycle formation of branched junction nanostructures, thereby generating numerous functional DNAzyme molecules for the production of colorimetric signal. On the basis of the results of gel electrophoresis and absorbance spectrophotometry, we can draw the conclusion that the dynamic assay protocol in the proposed colorimetric circuit is a reliable signal amplification strategy that functions as we designed.

Interrogation Capability of the Assay in Response to Different Target Concentrations. The dependence of sensing behavior of the proposed DNA nanodevice upon the different concentrations of target DNA was verified by the UV−visible absorbance of the solution under optimal conditions. (Experimental design for assay optimization can be found in Supporting Information, Section S1.) As depicted in Figure 2, the absorbance intensity at 414 nm increased

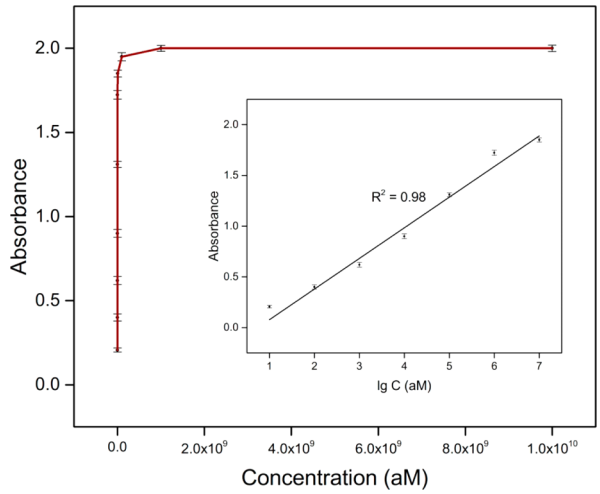

Figure 2. UV−vis absorbance curve of the sensing system in the presence of various concentration of target DNA. Inset: The corresponding calibration plot of the absorbance intensity vs logarithmic concentration of target DNA in the range from 10 aM to 10 pM. Error bars represent the standard deviation of three replicated experiments.

gradually with elevating target concentrations. The corresponding calibration curve (inset in Figure 2) displays that the absorbance values (Abs) are proportional to the logarithm of target concentration (lg C) with a dynamic range of 100 aM to 10 pM following a regression equation of Abs = 0.2952 lg C − 0.1795 (R^2 = 0.98). The detection sensitivity of the logical biosensor was calculated to be 100 aM based on three standard deviations (3σ) above the background signal (mean value of 10 negative controls), which is comparable to or superior over a considerable number of multiplexed analyzing tools.[11,18,33−35] Undoubtedly, the noticeable sensing performance was attributable to the uniquely designed triple signal amplification strategy, namely, AuNP-, DNA nanostructure-, and DNAzyme-assisted signal amplification technologies. The number of

DOI: 10.1021/acs.analchem.7b00607
Anal. Chem. 2017, 89, 6021−6028

loaded DNA oligonucleotides on a single AuNP directly correlates with the attainable signal intensity and biosensor sensitivity.[36−38] Recent studies have shown that implementing 30 nm nanoparticles yielded an approximately 200- to 600-fold signal enhancement for a given target recognition event.[39,40] The second signal amplification level originated from the exponential catalytic DNA hairpin self-assembly, which can provide a 50- to 100-fold signal amplification for the biosensor.[41−43] The automatic feedback amplification capability of the operation and further generation of numerous four-way junction nanostructures contributed the signal enhancement in this module. It should be noted that the motivation behind the selection of four-arm junctions in our design rather than three- or K-arm junctions was to maintain a balance between sensitivity and reaction time of the assay. Hence, biosensing with three-arm junctions provides a faster response time with lower sensitivity, while K-arm junctions confer a higher sensitivity with a long assay time.[30,41,44] After drawing the split partzymes of G-quadruplex together at each end of the four arms, intact G-quadruplex DNAzyme units were formed in the presence of hemin with peroxidase activity. According to our unified results with Deng et al., which merely used a 3:1 split mode of G-quadruplex peroxidase-mimicking DNAzyme for signal amplification,[45] it can be concluded that the DNAzyme can offer a 200- to 300-fold improvement in the sensitivity of the biosensor. The proposed nonenzymatic DNA circuit with the triple signal amplification would significantly enhance the overall sensitivity to 10^6−10^7-fold that rivals some enzymatic based-amplification methods.[46−50]

Feasibility of the Biosensor for Discrimination of Single Nucleotide Substitution (SNS). To inspect the selectivity of the biosensor, the absorbance values of the system were investigated against different input combinations. For this purpose, we utilized a perfect chimeric target DNA and three spurious targets containing SNS in *eae*, *rfbE*, and *fliC* biomarkers. For each perfect and spurious biomarker, Boolean values 1 (True) and 0 (False) were, respectively, allocated (Figure 3B). Accordingly, the chimeric target containing four perfect biomarkers was attributed a state 1,1,1,1 and the assay results for this state yielded a high absorbance value above the threshold (3σ above average of 10 negative controls is equal to 0.24). On the contrary, in the presence of only one spurious biomarker in each target (states (1,0,1,1), (1,0,1,1), and (1,1,1,0)), even in 100-fold excess of its concentration related to perfect chimeric target (1 pM), the absorbance intensity is lower than the threshold value (Figure 3A). These results clearly demonstrated that the proposed logical biosensor has an excellent discrimination capability for single nucleotide substitution. The great selectivity was attributed to the first AND gate of the circuit and several respective rigorous optimizing experiments to achieve the appropriate concentration and melting temperature of the biomarker-specific oligonucleotides for the best discrimination of SNS (data not shown). Beside single-nucleotide discrimination, another level of specificity can be obtained by using multiplex capability of the biosensors. Some of the biological functions or diseases are closely associated with various biomarkers such that a single biomarker is not sufficient for accurate diagnosis. Although nowadays the DNA microarray technology can accomplish the high-throughput and simultaneous analysis of multiple biomarkers,[51,52] its high cost, low sensitivity, and relatively low specificity, in terms of single-nucleotide discrimination, have been the major factors in preventing its widespread

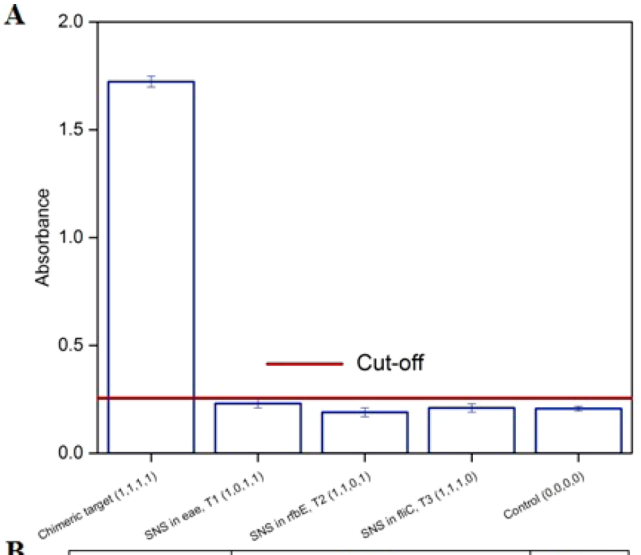

B

Sequence name	Intputs				Output
	16S rDNA	*eae* (T1)	*rfbE* (T2)	*fliC* (T3)	Green solution (naked eye evaluation)
Chimeric target	1	1	1	1	1
SNS in eae (T1)	1	0	1	1	0
SNS in rfbE (T2)	1	1	0	1	0
SNS in fliC (T3)	1	1	1	0	0
Control	0	0	0	0	0

Figure 3. (A) Assay selectivity of the presented DNA nanodevice toward 1 pM of target DNA and 100 pM of spurious targets containing SNS in *rfbE, fliC,* and *eae* biomarkers. Cut-off (threshold) absorbance value is measured based on 3σ role (0.24) to judge the output signals. (B) Corresponding truth table of the DNA logic circuit.

utilization.[53] The proposed DNA logic device not only allows single nucleotide discrimination, but it also expands the selectivity by applying a DNA domino chain to interrogate more than one biomarker simultaneously in each sample.

Real Sample Analysis. Fundamentally, all the advances in biosensor systems should be directed toward the practical approaches and the biosensing systems holding a potential for the reliable detection of an analyte in real biological samples are greatly appreciated. Within this concept, we investigated whether the proposed logical DNA biosensor has the analytical reliability and application potential for analysis of multiple biomarkers in genomic DNA. As a proof-of-concept, DNA extracted from four bacterial strains from *Enterobacteriacea* family, including *S. typhimurium* (contain 16S rDNA biomarker), *E. coli* O145 (contain 16S rDNA and T1 biomarkers), *E. coli* O55:H7 (contain 16S rDNA, T1 and T3 biomarkers), and *E. coli* O157:H7 (contain 16S rDNA, T1, T2, and T3 biomarkers) were assayed with the proposed strategy. Since, in the real sample experiments, the absorbance value for 10^9 CFU of spurious bacteria (*S. typhimurium, E. coli* O145, *E. coli* O55:H7) was higher than the threshold value of the assay (0.24), we set up the threshold value for real samples to 0.46 unit, based on the three standard deviations (3σ) above the mean absorbance value of a closely related bacterium (O55:H7). This threshold value sufficiently guarantees the accuracy of the assay for the detection of *E. coli* O157:H7 bacterium in the presence of high concentrations of spurious bacteria. As shown in Figure 4A, one can see that the signal of

DOI: 10.1021/acs.analchem.7b00607
Anal. Chem. 2017, 89, 6021−6028

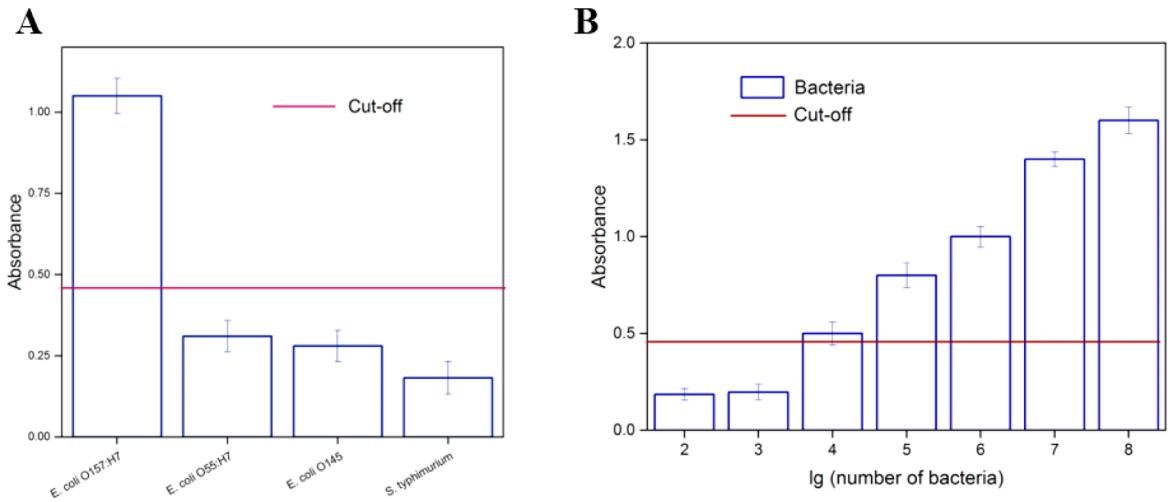

Figure 4. (A) Signal intensity of the proposed DNA nanodevice for interrogating four biomarkers in *E. coli* O157:H7, *E. coli* O55:H7, *E. coli* O145, and *S. typhimurium*. (B) Signal intensity of the system at 414 nm vs logarithm of numbers of *E. coli* O157:H7 cells.

the biosensor is significantly increased for DNA samples from *E. coli* O157:H7 bacterium, offering robust capability to monitor the simultaneous presence of the four biomarkers from genomic DNA. In contrast, for the other bacteria, there is only a slight increase of absorption compared to the *E. coli* O157:H7 samples (Figure 4A). These results confirm that all four biomarkers are present only in *E. coli* O157:H7 strains, which is in line with the previous reports.[54−56] Furthermore, the detection sensitivity for DNA extracted from serially diluted *E. coli* O157:H7 samples was calculated to be $\geq 10^4$ colonies forming units (CFU) (Figure 3B), which is comparable to or even better than several enzymatic assays.[56−59] It should be noted that the application of enzyme-free TMSD-based DNA circuits for analyzing target nucleic acid is not usually without challenges when the target molecules bear stable secondary structures.[37] In this condition, the target molecule is not easily hybridized to the circuit components and hence they reduce the efficiency of the sensing platform. This problem was addressed in the proposed DNA logic circuit by applying additional adaptor oligonucleotides, TR1, TR2, and TR3, with an optimized melting temperature. The adaptor oligonucleotides bind to the target DNA containing complicated secondary structures and translate the DNA hybridization events into structure-free sequences by their overhang region.[32] As a result, it can be concluded that the proposed smart DNA nanodevice could be reasonably applied in the simultaneous biomarker analysis for relevant clinical applications.

CONCLUSIONS

In summary, a DNA domino-based nanoscale logic circuit has been implemented as a smart biosensing platform for multiplexed analysis of nucleic acids. The logical nanodevice possesses three unique features: first, the nanodevice handles a triple signal amplification strategy, namely, AuNP-, DNA nanostructure-, and DNAzyme-assisted signal amplification technologies, providing an approximately 10^6−10^7-fold signal enhancement and a detection limit of 100 aM. Second, this technology engages additional adaptor oligonucleotides (TR1−TR3) with an optimized melting temperature to address the challenge associated with complicated secondary structures in the targets. Last, this nanodevice possesses potential ability to compute the presence of several continuous and/or discrete biomarker inputs by expanding the implemented DNA domino chain as a multiplexed platform. Furthermore, the biosensor can be easily reconfigured for multiplex analyses of other nucleic acid disease biomarkers. These practical properties would significantly benefit the modular computation approach and evoke promising potential applications in molecular computing, biosensing, and biotechnology.

ASSOCIATED CONTENT

Supporting Information

The Supporting Information is available free of charge on the ACS Publications website at DOI: 10.1021/acs.analchem.7b00607.

Oligonucleotide sequences and their related domains used in this study and the experimental design for the assay optimization (PDF)

AUTHOR INFORMATION

Corresponding Author

*Phone: +98 341 3222032. E-mail: ravan@uk.ac.ir.

ORCID

Hadi Ravan: 0000-0001-8560-4900

Notes

The authors declare no competing financial interest.

ACKNOWLEDGMENTS

The authors acknowledge financial support for this investigation by the Research Council of Shahid Bahonar University (Kerman, Iran).

REFERENCES

(1) Deshpande, A.; White, P. S. *Expert Rev. Mol. Diagn.* **2012**, *12*, 645−659.
(2) Meuzelaar, L. S.; Lancaster, O.; Pasche, J. P.; Kopal, G.; Brookes, A. J. *Nat. Methods* **2007**, *4*, 835−837.
(3) Pastinen, T.; Partanen, J.; Syvänen, A.-C. *Clin. Chem.* **1996**, *42*, 1391−1397.
(4) Shen, Y.; Wu, B.-L. *J. Genet. Genomics* **2009**, *36*, 257−265.
(5) Schena, M.; Heller, R. A.; Theriault, T. P.; Konrad, K.; Lachenmeier, E.; Davis, R. W. *Trends Biotechnol.* **1998**, *16*, 301−306.
(6) Hill, H. D.; Mirkin, C. A. *Nat. Protoc.* **2006**, *1*, 324.

DOI: 10.1021/acs.analchem.7b00607
Anal. Chem. 2017, 89, 6021−6028

(7) Pan, W.; Zhang, T.; Yang, H.; Diao, W.; Li, N.; Tang, B. *Anal. Chem.* **2013**, *85*, 10581−10588.
(8) Fan, D.; Zhu, J.; Liu, Y.; Wang, E.; Dong, S. *Nanoscale* **2016**, *8*, 3834−3840.
(9) Prigodich, A. E.; Randeria, P. S.; Briley, W. E.; Kim, N. J.; Daniel, W. L.; Giljohann, D. A.; Mirkin, C. A. *Anal. Chem.* **2012**, *84*, 2062−2066.
(10) Randeria, P. S.; Briley, W. E.; Chinen, A. B.; Guan, C. M.; Petrosko, S. H.; Mirkin, C. A. In *Nanotechnology-Based Precision Tools for the Detection and Treatment of Cancer*; Springer: Cham, Switzerland, 2015; pp 1−22.
(11) Lee, H.; Park, J.-E.; Nam, J.-M. *Nat. Commun.* **2014**, *5*, 3367.
(12) Fan, D.; Wang, E.; Dong, S. *ACS Appl. Mater. Interfaces* **2017**, *9*, 1322−1330.
(13) Fan, D.; Zhu, J.; Zhai, Q.; Wang, E.; Dong, S. *Chem. Commun.* **2016**, *52*, 3766−3769.
(14) Fan, D.; Wang, E.; Dong, S. *Nano Res.* **2017**, 1−10.
(15) Feng, L.; Lyu, Z.; Offenhäusser, A.; Mayer, D. *Angew. Chem., Int. Ed.* **2015**, *54*, 7693−7697.
(16) Qian, L.; Winfree, E. *Science* **2011**, *332*, 1196−1201.
(17) Hemphill, J.; Deiters, A. *J. Am. Chem. Soc.* **2013**, *135*, 10512−10518.
(18) Liu, X.; Aizen, R.; Freeman, R.; Yehezkeli, O.; Willner, I. *ACS Nano* **2012**, *6*, 3553−3563.
(19) Kang, D.; White, R. J.; Xia, F.; Zuo, X.; Vallée-Bélisle, A.; Plaxco, K. W. *NPG Asia Mater.* **2012**, *4*, e1.
(20) Pu, F.; Liu, Z.; Ren, J.; Qu, X. *Chem. Commun.* **2013**, *49*, 2305−2307.
(21) Pu, F.; Liu, Z.; Yang, X.; Ren, J.; Qu, X. *Chem. Commun.* **2011**, *47*, 6024−6026.
(22) Lin, H.-Y.; Chen, J.-Z.; Li, H.-Y.; Yang, C.-N. *Sci. Rep.* **2015**, *5*, 2045−2322.
(23) Rana, M.; et al. *Chem. Commun.* **2016**, *52*, 3524−3527.
(24) Ravan, H. *Anal. Chim. Acta* **2016**, *910*, 68−74.
(25) Fan, D.; Wang, E.; Dong, S. *Chemical Science* **2017**, *8*, 1888−1895.
(26) Mailloux, S.; Gerasimova, Y. V.; Guz, N.; Kolpashchikov, D. M.; Katz, E. *Angew. Chem., Int. Ed.* **2015**, *54*, 6562−6566.
(27) Zhu, J.; Li, T.; Zhang, L.; Dong, S.; Wang, E. *Biomaterials* **2011**, *32*, 7318−7324.
(28) Gao, W.; Zhang, L.; Zhang, Y.-M.; Liang, R.-P.; Qiu, J.-D. *J. Phys. Chem. C* **2014**, *118*, 14410−14417.
(29) Chen, J.; Zhou, S.; Wen, J. *Angew. Chem., Int. Ed.* **2015**, *54*, 446−450.
(30) Zhou, W.; Liang, W.; Li, X.; Chai, Y.; Yuan, R.; Xiang, Y. *Nanoscale* **2015**, *7*, 9055−9061.
(31) Ravan, H.; Yazdanparast, R. *Anal. Chim. Acta* **2012**, *733*, 64−70.
(32) Ravan, H. *TrAC, Trends Anal. Chem.* **2015**, *65*, 97−106.
(33) Bi, S.; Ye, J.; Dong, Y.; Li, H.; Cao, W. *Chem. Commun.* **2016**, *52*, 402−405.
(34) Jin, Z.; Geißler, D.; Qiu, X.; Wegner, K. D.; Hildebrandt, N. *Angew. Chem., Int. Ed.* **2015**, *54*, 10024−10029.
(35) Chen, S.; Chu, L. T.; Yeung, P. P.; Zhao, Z.; Bao, Y.; Chan, M. S.; Lo, P. K.; Chen, T.-H. *ACS Appl. Mater. Interfaces* **2015**, *7*, 22821−22830.
(36) Zhang, J.; Song, S.; Wang, L.; Pan, D.; Fan, C. *Nat. Protoc.* **2007**, *2*, 2888−2895.
(37) Ravan, H. *Biosens. Bioelectron.* **2016**, *80*, 67−73.
(38) Ravan, H.; Kashanian, S.; Sanadgol, N.; Badoei-Dalfard, A.; Karami, Z. *Anal. Biochem.* **2014**, *444*, 41−46.
(39) Hurst, S. J.; Lytton-Jean, A. K.; Mirkin, C. A. *Anal. Chem.* **2006**, *78*, 8313−8318.
(40) Zhang, J.; Song, S.; Zhang, L.; Wang, L.; Wu, H.; Pan, D.; Fan, C. *J. Am. Chem. Soc.* **2006**, *128*, 8575−8580.
(41) Yin, P.; Choi, H. M.; Calvert, C. R.; Pierce, N. A. *Nature* **2008**, *451*, 318−322.
(42) Jung, C.; Ellington, A. D. *Acc. Chem. Res.* **2014**, *47*, 1825−1835.
(43) Li, B.; Ellington, A. D.; Chen, X. *Nucleic Acids Res.* **2011**, *39*, e110−e110.
(44) Chen, J.; Wen, J.; Yang, G.; Zhou, S. *Chem. Commun.* **2015**, *51*, 12373−12376.
(45) Deng, M.; Zhang, D.; Zhou, Y.; Zhou, X. *J. Am. Chem. Soc.* **2008**, *130*, 13095−13102.
(46) Compton, J. *Nature* **1991**, *350*, 91−92.
(47) Walker, G. T.; Fraiser, M. S.; Schram, J. L.; Little, M. C.; Nadeau, J. G.; Malinowski, D. P. *Nucleic Acids Res.* **1992**, *20*, 1691−1696.
(48) Vincent, M.; Xu, Y.; Kong, H. *EMBO Rep.* **2004**, *5*, 795−800.
(49) Van Ness, J.; Van Ness, L. K.; Galas, D. J. *Proc. Natl. Acad. Sci. U. S. A.* **2003**, *100*, 4504−4509.
(50) Pemov, A.; Modi, H.; Chandler, D.; Bavykin, S. *Nucleic Acids Res.* **2005**, *33*, e11−e11.
(51) Castoldi, M.; Schmidt, S.; Benes, V.; Hentze, M. W.; Muckenthaler, M. U. *Nat. Protoc.* **2008**, *3*, 321−329.
(52) Lee, J. M.; Jung, Y. *Angew. Chem., Int. Ed.* **2011**, *50*, 12487−12490.
(53) Zhou, Y.; Zhang, J.; Zhao, L.; Li, Y.; Chen, H.; Li, S.; Cheng, Y. *ACS Appl. Mater. Interfaces* **2016**, *8*, 1520−1526.
(54) Ravan, H.; Amandadi, M.; Sanadgol, N. *Microb. Pathog.* **2016**, *91*, 161−165.
(55) Ravan, H.; Amandadi, M. *Curr. Microbiol.* **2015**, *71*, 274−282.
(56) Yaron, S.; Matthews, K. *J. Appl. Microbiol.* **2002**, *92*, 633−640.
(57) Zoetendal, E. G.; Ben-Amor, K.; Akkermans, A. D.; Abee, T.; De Vos, W. M. *Syst. Appl. Microbiol.* **2001**, *24*, 405−410.
(58) Holland, J.; Louie, L.; Simor, A.; Louie, M. *J. Clin. Microbiol.* **2000**, *38*, 4108−4113.
(59) Call, D. R.; Brockman, F. J.; Chandler, D. P. *Int. J. Food Microbiol.* **2001**, *67*, 71−80.

DOI: 10.1021/acs.analchem.7b00607
Anal. Chem. 2017, 89, 6021−6028